Structure and Organization of Hemolytic and Nonhemolytic Diastereomers of Antimicrobial Peptides in Membranes†

Jiang Hong,‡ Ziv Oren,‡ and Yechiel Shai*

Department of Biological Chemistry, Weizmann Institute of Science, Rehovot, 76100 Israel

Received August 9, 1999; Revised Manuscript Received October 8, 1999

ABSTRACT: Recently, we reported on a new group of diastereomers of short-model peptides (12 amino acids long) composed of leucine and lysine with varying ratios, possessing several properties that make them potentially better than native or de novo-designed all L-amino acid antimicrobial peptides. Preliminary studies have revealed that modulating the hydrophobicity and positive charges of these diastereomers is sufficient to confer antibacterial activity and cell selectivity. However, the relationship between their biological function, structure, and mode of action was not investigated. Here we synthesized and investigated three types of linear model diastereomers (12 amino acids long) with varying lysine:leucine (or tryptophan) ratios (i.e., K_3L_8W, K_5L_6W, and K_7L_4W), which confer different levels of lytic activities. For each K:L ratio, tryptophan was introduced in the middle or the N- or C-terminus of the peptides, as an intrinsic fluorescent probe. Only the hemolytic peptide K_3L_8W binds to both negatively charged and zwitterionic phospholipid membranes. K_5L_6W and K_7L_4W bind similarly, but only to negatively charged membranes, despite the fact that K_5L_6W is substantially more lytic to bacteria than K_7L_4W. Interestingly, although K_3L_8W contains 33% D-amino acids, ATR-FTIR spectroscopy revealed a structure of ∼90% α-helix in both types of membranes. In addition, K_5L_6W contains ∼40% 3_{10}-helix and K_7L_4W is predominantly a random coil in membranes. Polarized ATR-FTIR and tryptophan-quenching experiments, using brominated phospholipids, revealed a similar depth of penetration and an orientation that was parallel to the membrane surface for all the peptides, but with K_3L_8W affecting the lipid order more than the others. The results provide insight into the mode of action of this group of diastereomeric peptides, and the effect of hydrophobicity and positive charges on their membrane structure, function, and cell selectivity. Moreover, this research should assist in the development of suitable diastereomeric peptide antibiotics for therapeutic use that would overcome the problem the increasing resistance of bacteria to conventional antibiotics.

Antimicrobial resistance to conventional antibiotics has become a major problem worldwide because of their extensive use. In fact, strains of bacteria already exist that are resistant to all available antibiotics (*1*, *2*). The development of new families of antibiotics that can overcome the resistance problem has become a very important task. One such major family consists of the antimicrobial peptides. Antimicrobial peptides are natural antibiotics that constitute a major part of the innate immunity of a wide range of organisms, including humans (*3*−*9*). During the past two decades, numerous studies have demonstrated the essential role of antimicrobial peptides as the first line of defense against invading pathogens and their uncontrolled proliferation. An important property of most antimicrobial peptides is their ability to selectively kill bacteria but not normal eukaryotic cells. Many studies indicated that a specific secondary structure is required and that the common feature found in most of them are an amphipathic character and a net positive charge. Most of the studies were carried out with linear amphipathic α-helical cytolytic peptides (≤40 amino acids) from a host-defense system (*3*). These polypeptides vary considerably in chain length, hydrophobicity, and overall distribution of charges, but share a common structure upon association with lipid bilayers, namely, an amphipathic α-helix structure (*10*, *11*). This group includes (i) lytic peptides that are toxic only to microorganisms, e.g., cecropins isolated from the cecropia moth (*12*) and magainins (*13*) and dermaseptins (*14*) isolated from the skin of frogs; (ii) lytic peptides that lyse mammalian cells, such as δ-hemolysin isolated from *Staphylococcus aureus* (*15*); and (iii) non-cell-selective lytic peptides, such as the bee venom melittin (*16*) and the neurotoxin pardaxin (*17*, *18*), that can lyse microorganisms and mammalian cells.

Most of the antimicrobial peptides are composed of L-amino acids with a defined α-helix or β-sheet secondary structure. Another important group of peptide antibiotics composed of both L- and D-amino acids includes gramicidins, actinomycins, bacitracin, polymyxins, lantibiotics, and bombinins H 3−5 (*19*, *20*). The coexistence of L- and D-amino acids leads to unique structures and properties that are completely different from those of all other L-peptides. For example, the gramicidins (*21*) are composed of alternating L- and D-amino acids, forming a β-type of helix with a

† This research was supported by the Israel Academy of Sciences and Humanities.

* To whom correspondence should be addressed: Department of Biological Chemistry, The Weizmann Institute of Science, Rehovot, 76100 Israel. Telephone: 972-8-9342711. Fax: 972-8-9344112. E-mail: bmshai @weizmann.weizmann.ac.il.

‡ These authors contributed equally to this study.

10.1021/bi991850y CCC: $18.00
Published on Web 11/25/1999

hydrogen bond pattern of the backbone similar to that in β-sheets. In these β-helices, the amino acid residues point outward and the carbonyl moieties alternately point upward and downward within the helix, providing the helices with a hydrophilic pore. Unfortunately, these peptide antibiotics are not cell-selective and are highly toxic to normal eukaryotic cells.

Recently, we have incorporated several D-amino acids into the α-helical cytolytic peptides pardaxin (*22*) and melittin (*23*). Although the resulting diastereomers lost their cytotoxic effects on mammalian cells, they retained high antibacterial activity, thus providing a basis for designing novel peptide antibiotics composed of D- and L-amino acids that are selective to microorganisms. On the basis of these studies and those carried out with all L-amino acids model peptides (*24*, *25*), we designed and investigated short-model peptides (12 amino acids long), composed of only leucine and lysine with varying ratios, and one-third of their sequence consisted of D-amino acids (*26*). Studies of their function revealed that modulating the ratio between the hydrophobicity and a positive charge is sufficient to confer antibacterial activity and cell selectivity. A highly hydrophobic diastereomer was used to lyse the eukaryotic and prokaryotic cells. In contrast, a very positively charged diastereomer had low antibacterial activity and could not lyse the eukaryotic cells. In the boundary between the high hydrophobicity and high positive charge of the diastereomers, we noted selective and potent antibacterial activity. However, the structure and organization in phospholipid membranes of the diastereomers, as well as their ability to bind to phospholipids of different compositions, have not yet been studied. Knowing this information may extend our knowledge of the mechanism by which diastereomers of non-cell-selective lytic peptides can discriminate between different organisms and, consequently, provide a better tool for designing potent diastereomeric antimicrobial peptides.

In this study, we focused on three types of diastereomers: (i) hemolytic peptides with high antibacterial activity, (ii) nonhemolytic peptides with high antibacterial activity, and (iii) nonhemolytic peptides with poor antibacterial activity. In each type of diastereomer, tryptophan was introduced in the middle or the N- or C-terminus of the peptides. The peptides were then characterized with regard to their biological function and binding to model phospholipid membranes. The secondary structure of the peptides in zwitterionic (PC[1]/cholesterol) and negatively charged (PE/PG) phospholipid membranes, and their ability to perturb the lipid order, were studied using attenuated total reflectance Fourier transform infrared (ATR-FTIR) spectroscopy. In addition, the depth of their penetration into phospholipid membranes was estimated by using tryptophan quenching in the presence of brominated phospholipids. The structure, orientation, and depth of penetration of the diastereomers into membranes provided insight into their mode of action and the effect of hydrophobicity and positive charges on their function and selectivity.

[1] Abbreviations: ATR-FTIR, attenuated total reflectance Fourier transform infrared; BHA, 4-methyl benzhydrylamine resin; Boc, butyloxycarbonyl; CFU, colony-forming units; HF, hydrogen fluoride; hRBC, human red blood cells; MIC, minimal inhibitory concentration; PBS, phosphate-buffered saline; PC, egg phosphatidylcholine; PE, *E. coli* phosphatidylethanolamine; PG, egg phosphatidylglycerol; RP-HPLC, reverse phase high-performance liquid chromatography; SUV, small unilamellar vesicles; TFA, trifluoroacetic acid.

MATERIALS AND METHODS

Materials. 4-Methyl benzhydrylamine resin (BHA) and butyloxycarbonyl (Boc) amino acids were purchased from Calibochem-Novabiochem (La Jolla, CA). Other reagents used for peptide synthesis included trifluoroacetic acid (TFA, Sigma), *N*,*N*-diisopropylethylamine (DIEA, Aldrich, distilled over ninhydrin), dicyclohexylcarbodiimide (DCC, Fluka), 1-hydroxybenzotriazole (HOBT, Pierce), and dimethylformamide (peptide synthesis grade, Biolab). Egg phosphatidylcholine (PC) was purchased from Lipid Products (South Nutfield, U.K.). Egg phosphatidylglycerol (PG) and phosphatidylethanolamine (PE) (type V, from *Escherichia coli*) were purchased from Sigma. Cholesterol (extra pure) was supplied by Merck (Darmstadt, Germany) and recrystallized twice from ethanol. All other reagents were analytical grade. Buffers were prepared in doubly glass-distilled water.

Peptide Synthesis and Purification. Peptides were synthesized by a solid-phase method on 4-methyl benzhydrylamine resin (0.05 mequiv) (*27*). The resin-bound peptides were cleaved from the resins by hydrogen fluoride (HF), and after HF evaporation extracted with dry ether. HF cleavage of the peptides bound to 4-methyl benzhydrylamine resin resulted in C-terminally amidated peptides. These crude peptide preparations contained one major peak, as revealed by RP-HPLC, that was 60−80% pure peptide by weight. The synthesized peptides were further purified by RP-HPLC on a C_{18} reverse phase Bio-Rad semipreperative column (250 mm × 10 mm, 300 Å pore size, 5 μm particle size). The column was eluted over the course of 40 min, using a linear gradient of 10 to 60% acetonitrile in water, both containing 0.05% TFA (v/v), at a flow rate of 1.8 mL/min. The purified peptides, which were shown to be homogeneous (∼95%) by analytical HPLC, were subjected to amino acid analysis to confirm their content.

Preparation of Liposomes. Small unilamellar vesicles (SUV) were prepared by sonication of PC/cholesterol (10:1 w/w) or PE/PG (7:3 w/w) dispersions. Briefly, dry lipid and cholesterol (10:1 w/w) were dissolved in a $CHCl_3$/MeOH mixture (2:1 v/v). The solvents were then evaporated under a stream of nitrogen, and the lipids (at a concentration of 7.2 mg/mL) were subjected to a vacuum for 1 h and then resuspended in the appropriate buffer, by vortexing. The resultant lipid dispersions were then sonicated for 5−15 min in a bath type sonicator (G1125SP1 sonicator, Laboratory Supplies Company Inc.) until they were clear. To avoid degradation of unsaturated lipids, sonication was performed at ∼10 °C under a nitrogen atmosphere. The lipid concentrations of the resulting preparations were determined by phosphorus analysis (*28*). Vesicles were visualized using a JEOL JEM 100B electron microscope (Japan Electron Optics Laboratory Co., Tokyo, Japan) as follows. A drop of vesicles was deposited on a carbon-coated grid and negatively stained with uranyl acetate. Examination of the grids demonstrated that the vesicles were unilamellar with an average diameter of 20−50 nm.

Antibacterial Activity of the Peptides. The antibacterial activity of the peptides was examined in sterile 96-well plates (Nunc F96 microtiter plates) in a final volume of 100 μL as

follows. Aliquots (50 μL) of a suspension containing bacteria at a concentration of 10^6 colony-forming units (CFU)/mL in culture medium (LB medium) were added to 50 μL of water containing the peptide in serial 2-fold dilutions in water. The extent of inhibition of growth was determined by measuring the absorbance at 492 nm with a Microplate autoreader El309 (Bio-tek Instruments), after incubation for 18−20 h at 37 °C. Antibacterial activities were expressed as the minimal inhibitory concentration (MIC), the concentration at which 100% inhibition of growth was observed after incubation for 18−20 h. The bacteria that were used included *E. coli* D21, *Acinetobacter calcoaceticus* Ac11, *Bacillus megaterium* Bm11, and *Bacillus subtilis* ATCC 6051.

Hemolysis of Human Red Blood Cells. The peptides were tested for their hemolytic activity against human red blood cells (hRBC). Fresh hRBC with EDTA were rinsed three times with PBS [35 mM phosphate buffer and 0.15 M NaCl (pH 7.3)] by centrifugation for 10 min at 800*g* and resuspended in PBS. Peptides dissolved in PBS were then added to 50 μL of a solution of the stock hRBC in PBS to reach a final volume of 100 μL (final erythrocyte concentration, 5% v/v). The resulting suspension was incubated under agitation for 30 min at 37 °C. The samples were then centrifuged at 800*g* for 10 min. Release of hemoglobin was monitored by measuring the absorbance of the supernatant at 540 nm. Controls for zero hemolysis (blank) and 100% hemolysis consisted of hRBC suspended in PBS and 1% Triton, respectively.

Binding of Peptides to Vesicles. The interaction of the peptides with vesicles consisting of mixtures of zwitterionic phospholipids and cholesterol (PC/cholesterol) or zwitterionic and negatively charged phospholipids (PE/PG) was characterized by measuring changes in the emission intensity of the peptides' intrinsic tryptophan in SUV titration experiments. Briefly, SUV were added to a fixed amount of peptide (0.5 μM) dissolved in PBS (35 mM phosphate buffer and 0.15 M NaCl) at pH 6.8 and 24 °C. A 1 cm path length quartz cuvette that had a final reaction volume of 2 mL was used in all experiments. The fluorescence intensity was measured as a function of the lipid:peptide molar ratio (four separate experiments) on a SLM-Aminco, Series 2 spectrofluorimeter, with excitation set at 280 nm, using a 4 nm slit, and emission set at 340 nm, using a 4 nm slit. The binding isotherms were analyzed as a partition equilibrium, using the following formula (*29*, *30*):

$$X_b = K_P C_f$$

where X_b is defined as the molar ratio of bound peptide (C_b) per total lipid (C_L), K_P corresponds to the partition coefficient, and C_f represents the equilibrium concentration of the free peptide in solution. For practical purposes, it was assumed that the peptides initially were partitioned only over the outer leaflet (60%) of the SUV (*31*). Therefore, the partition equation becomes

$$X_b^* = K_P^* C_f$$

where X_b^* is defined as the molar ratio of bound peptide per 60% of total lipid and K_P^* is the estimated surface partition constant. The curve resulting from plotting X_b^* versus C_f is termed the conventional binding isotherm.

ATR-FTIR Measurements. Spectra were obtained with a Bruker equinox 55 FTIR spectrometer equipped with a deuterated triglyceride sulfate (DTGS) detector and coupled with an ATR device. For each spectrum, 200 or 300 scans were collected, with a resolution of 4 cm^{-1}. During data acquisition, the spectrometer was continuously purged with dry N_2 to eliminate the spectral contribution of atmospheric water. Samples were prepared as previously described (*32*). Briefly, a mixture of PC/cholesterol (10:1 w/w, 1.25 mg) or PE/PG (7:3 w/w,1.25 mg) alone or with peptide (~24 μg) was deposited on a ZnSe horizontal ATR prism (80 mm × 7 mm). The aperture angle of 45° yielded 25 internal reflections. Before sample preparation, the trifluoroacetate (CF_3COO^-) counterions which strongly associate to the peptide were replaced with chloride ions through several lyophilizations of the peptides in 0.1 M HCl. This allowed the elimination of the strong C═O stretching absorption band near 1673 cm^{-1} (*33*). Lipid/peptide mixtures were prepared by dissolving them together in a 1:2 MeOH/CH_2Cl_2 mixture and drying under a stream of dry nitrogen while moving a Teflon bar back and forth along the ZnSe prism. Polarized spectra were recorded, and the respective pure phospholipid contribution in each polarization was subtracted to yield the difference spectra. The background for each spectrum was a clean ZnSe prism. Hydration of the sample was achieved by introduction of excess deuterium oxide (^2H_2O) into a chamber placed on top of the ZnSe prism in the ATR casting and incubation for 2 h prior to acquisition of spectra. H−D exchange was considered complete due to the complete shift of the amide II band. Any contribution of ^2H_2O vapor to the absorbance spectra near the amide I peak region was eliminated by subtraction of the spectra of pure lipids equilibrated with ^2H_2O under the same conditions.

ATR-FTIR Data Analysis. Prior to curve fitting, a straight baseline passing through the ordinates at 1700 and 1600 cm^{-1} was subtracted. To resolve overlapping bands, the spectra were processed using PEAKFIT (Jandel Scientific, San Rafael, CA). Second-derivative spectra accompanied by 13-data point Savitsky−Golay smoothing were calculated to identify the positions of the component bands in the spectra. These wavenumbers were used as initial parameters for curve fitting with Gaussian component peaks. The position, bandwidths, and amplitudes of the peaks were varied until (i) the resulting bands shifted by no more than 2 cm^{-1} from the initial parameters, (ii) all the peaks had reasonable half-widths (<20−25 cm^{-1}), and (iii) good agreement between the calculated sum of all components and the experimental spectra was achieved ($r^2 > 0.99$). The relative contents of different secondary structure elements were estimated by dividing the areas of individual peaks, assigned to particular secondary structure, by the whole area of the resulting amide I band. The results of four independent experiments were averaged.

Analysis of the Polarized ATR-FTIR Spectra. The ATR electric fields of incident light were calculated as follows (*34*, *35*).

$$E_x = \frac{2\cos\theta\sqrt{\sin^2\theta - {n_{21}}^2}}{\sqrt{(1-{n_{21}}^2)[(1+{n_{21}}^2)\sin^2\theta - {n_{21}}^2]}}$$

$$E_y = \frac{2\cos\theta}{\sqrt{1-{n_{21}}^2}}$$

$$E_z = \frac{2\sin\theta\cos\theta}{\sqrt{(1-{n_{21}}^2)[(1+{n_{21}}^2)\sin^2\theta - {n_{21}}^2]}}$$

where θ is the angle of a light beam to the prism normal at the point of reflection (45°) and $n_{21} = n_2/n_1$ [n_1 and n_2 are the refractive indices of ZnSe (taken as 2.4) and the membrane sample (taken as 1.5), respectively]. Under these conditions, E_x, E_y, and E_z are 1.09, 1.81, and 2.32, respectively. The electric field components together with the dichroic ratio [defined as the ratio between absorption of parallel (to a membrane plane), A_p, and perpendicularly polarized incident light, A_s] are used to calculate the orientation order parameter, f, by the following formula:

$$R^{ATR} = \frac{A_p}{A_s} = \frac{{E_x}^2}{{E_y}^2} + \frac{\frac{{E_z}^2}{{E_y}^2}\left(f\cos^2\alpha + \frac{1-f}{3}\right)}{\frac{f\sin^2\alpha}{2} + \frac{1-f}{3}}$$

where α is the angle between the transition moment of the amide I vibration of an α-helix and the helix axis. Several values ranging from 27° to 40° were reported for α in the literature (*36*). We used the values of 27° (*35*, *37*) and 39° (*38*, *39*) for α. Lipid order parameters were obtained from the symmetric (~2853 cm^{-1}) and antisymmetric (~2922 cm^{-1}) lipid stretching mode using the same equations, setting α equal to 90° (*35*).

Tryptophan-Quenching Experiments. Tryptophan which is sensitive to its environment has been utilized previously in combination with brominated phospholipids (Br-PC) to evaluate peptide localization in the membrane (*40*, *41*). Br-PC used as quenchers of tryptophan fluorescence are suitable for probing the membrane insertion of peptides, since they act over a short distance and do not drastically perturb the membrane. The diastereomers, each of which contains one tryptophan residue, were added (final concentration of 0.5 μM) to 2 mL of PBS buffer [35 mM phosphate buffer and 0.15 M NaCl (pH 7.3)] containing 15 μL (60 μM) of Br-PC/PE/PG (2.5:4.5:3 w/w) SUV, thus establishing a lipid:peptide ratio of 120:1. After incubation for 2 min at room temperature, an emission spectrum of the tryptophan was recorded using a SLM-Aminco Series 2 spectrofluorometer, with excitation set at 280 nm (4 nm slit). SUV composed of Br-PC, PE, and PG (2.5:4.5:3 w/w) which contained either 6,7-Br-PC, 9,10-Br-PC, or 11,12-Br-PC were used. Three separate experiments were conducted for each diastereomer. In control experiments, PC/PE/PG (2.5:4.5:3 w/w) SUV without Br-PC were used.

RESULTS

Three groups of 12-amino acid diastereomers of model peptides were synthesized. They are composed of positively charged (lysine) and hydrophobic (leucine and tryptophan) amino acids with three varying ratios: 3:9, 5:7, and 7:5. The location of D-amino acids remained constant with all of the peptides. In each group, a leucine was substituted with the hydrophobic amino acid tryptophan at either the middle of the peptide or its N- or C-terminus, to maintain the ratio between the positively charged and the hydrophobic amino acids. Tryptophan was then used as an intrinsic fluorescent probe for spectrofluorometric studies. Table 1 shows the sequences of the peptides and their designations, net charges, and hydrophobicities (*42*).

Antibacterial and Hemolytic Activity of the Peptides. Antibacterial and hemolytic activities of the peptides were tested to verify that the incorporation of tryptophan at different positions along the peptide chain did not significantly affect their function. The antibiotic tetracycline served as a control in the antibacterial assay. Table 2 gives the MIC for a representative set of test bacteria, which includes two Gram-negative species (*E. coli* and *A. calcoaceticus*) and two Gram-positive species (*B. megaterium* and *B. subtilis*). Table 2 also shows the percentage of hemolysis caused by applying the peptides at a concentration of 50 μM. The data revealed that within each group, the incorporation of tryptophan at the different positions did not substantially affect their biological function. The analogues of $[D]L^{3,4,8,10}$-K_3L_8W, the most hydrophobic group, were not cell-selective, and could lyse both erythrocytes and bacteria, whereas the analogues of the $[D]L^{3,4,8,10}$-K_5L_6W group were nonhemolytic but lysed bacteria with high potency. The most hydrophilic group of analogues, $[D]L^{3,4,8,10}$-K_7L_4W, were also cell-selective, but exhibited the lowest antibacterial activity. Interestingly, this analogue was still highly potent only on *B. megaterium* with a potency similar to those of the others.

Interaction of the Peptides with Phospholipid Membranes. Since the biological functions of the three analogues of each group were similar, only $[D]L^{3,4,8,10}$-K_3L_8W(m), $[D]L^{3,4,8,10}$-K_5L_6W(m), and $[D]L^{3,4,8,10}$-K_7L_4W(m) were further investigated for their structure and mode of action with model phospholipid membranes. However, all of the nine analogues were used in the tryptophan-quenching experiments.

Binding Studies. The selective cytolytic activity of the diastereomers may be due to their inability to bind different phospholipid membranes, or alternatively, they may bind, but once bound cannot organize themselves into structures that induce membrane lysis. To distinguish between these two possibilities, we conducted a binding study. The single tryptophan residue at position 6 of $[D]L^{3,4,8,10}$-K_3L_8W(m), $[D]L^{3,4,8,10}$-K_5L_6W(m), and $[D]L^{3,4,8,10}$-K_7L_4W(m) was used as an intrinsic fluorescence probe to follow the binding of the peptides to model phospholipid membranes. PE/PG (7:3 w/w), a phospholipid composition typical of *E. coli* (*43*), and the zwitterionic PC/cholesterol (10:1 w/w), a phospholipid composition used for mimicking the major components of the outer leaflet of human erythrocytes (*44*), were used in the binding assays. A fixed concentration (0.5 μM) of the peptide was titrated using the desired vesicles (PE/PG or PC), and an increase in the fluorescence intensity was observed when binding occurred. Plotting of the resulting increases in the fluorescence intensities of tryptophan as a function of lipid:peptide molar ratios yielded conventional binding curves. The binding curves of all the diastereomers with PE/PG show that saturation occurred at a lipid:peptide molar ratio of ~100:1 (Figure 1A). The binding isotherms were

Table 1: Sequences, Designations, Net Charges, and Hydrophobicities of the Peptides That Were Investigated

peptide	sequence[a,b]	net charge	hydrophobicity[c]
[D]L^{3,4,8,10}-K$_3$L$_8$W(n)	K W **L L** L L K **L** L **L** L K-NH$_2$	+4	0.11
[D]L^{3,4,8,10}-K$_3$L$_8$W(m)	K L **L L** L W K **L** L **L** L K-NH$_2$	+4	0.11
[D]L^{3,4,8,10}-K$_3$L$_8$W(c)	K L **L L** L L K **L** L **L** W K-NH$_2$	+4	0.11
[D]L^{3,4,8,10}-K$_5$L$_6$W(n)	K W **L L** K L K **L** K **L** L K-NH$_2$	+6	0.16
[D]L^{3,4,8,10}-K$_5$L$_6$W(m)	K L **L L** K W K **L** K **L** L K-NH$_2$	+6	0.16
[D]L^{3,4,8,10}-K$_5$L$_6$W(c)	K L **L L** K L K **L** K **L** W K-NH$_2$	+6	0.16
[D]L^{4,8,10}-K$_7$L$_4$W(n)	K K **W L** K L K **L** K **L** K K-NH$_2$	+8	0.43
[D]L^{3,4,8,10}-K$_7$L$_4$W(m)	K K **L L** K W K **L** K **L** K K-NH$_2$	+8	0.43
[D]L^{3,4,8}-K$_7$L$_4$W(c)	K K **L L** K L K **L** K **W** K K-NH$_2$	+8	0.43

[a] Underlined and bold amino acids are D-enantiomers. [b] The C-terminus is amidated. [c] Mean values of hydrophobicity were calculated using the consensus value of hydrophobicity scale (*43*).

Table 2: Minimal Inhibitory Concentrations of the Peptides

	minimal inhibitory concentration[a] (μM)				
peptide	*E. coli* (D21)	*A. calcoaceticus* (Ac11)	*B. megaterium* (Bm11)	*B. subtilis* (ATCC 6051)	% hemolysis at 50 μM peptide
[D]L^{3,4,8,10}-K$_3$L$_8$Wn	6.5	3.5	0.8	1.5	31
[D]L^{3,4,8,10}-K$_3$L$_8$Wm	4.5	4.5	1	1.3	39.4
[D]L^{3,4,8,10}-K$_3$L$_8$Wc	6.5	6	1	1.6	44.2
[D]L^{3,4,8,10}-K$_5$L$_6$Wn	10	8.5	0.5	1.8	0
[D]L^{3,4,8,10}-K$_5$L$_6$Wm	8.5	8.5	0.6	2.5	0
[D]L^{3,4,8,10}-K$_5$L$_6$Wc	8	9.5	0.6	2	0
[D]L^{4,8,10}-K$_7$L$_4$Wn	140	230	0.7	90	0
[D]L^{3,4,8,10}-K$_7$L$_4$Wm	120	200	0.6	100	0
[D]L^{3,4,8}-K$_7$L$_4$Wc	130	220	1	110	0
tetracycline	1.5	1.5	1.2	6.5	

[a] Results are the means of three independent experiments each performed in duplicate, with standard deviations not exceeding 25%.

constructed by plotting X_b* (the molar ratio of bound peptide per 60% of the total lipid) versus C_f (the equilibrium concentration of the free peptide in the solution) and are shown in Figure 1B. The surface partition coefficients were estimated by extrapolating the initial slopes of the curves to C_f values of zero. Table 3 summarizes the estimated surface partition coefficients, K_p*, of the diastereomers. The data reveal that there is no major difference between the binding properties of the peptides. This can explain the similar potencies of [D]L^{3,4,8,10}-K$_3$L$_8$W(m) and [D]L^{3,4,8,10}-K$_5$L$_6$W-(m), but cannot explain the finding that [D]L^{3,4,8,10}-K$_7$L$_4$W-(m) is almost inactive.

Binding studies with PC vesicles revealed no net increase in the tryptophan fluorescence of [D]L^{3,4,8,10}-K$_5$L$_6$W(m) and [D]L^{3,4,8,10}-K$_7$L$_4$W(m), or blue shifts in their emission spectrum up to the maximal lipid:peptide molar ratio that was tested (400:1). This indicates that the diastereomers do not bind to PC vesicles or, alternatively, bind very weakly. However, a blue shift in the emission spectrum from 353 nm in solution to 345 nm in the presence of PC was observed with [D]L^{3,4,8,10}-K$_3$L$_8$W(m), indicating that this diastereomer binds PC vesicles. Since no net increase in the fluorescence was observed up to the maximal lipid:peptide molar ratio that was tested (400:1), it was not possible to derive the corresponding binding isotherm. A possible explanation for this result is that [D]L^{3,4,8,10}-K$_3$L$_8$W(m) self-associates upon binding to PC vesicles. The location of the tryptophan residue, within an aggregate, may confine the changes in the fluorescence intensity while allowing the blue shift to occur.

The shape of the binding isotherm of a peptide can provide information about the organization of the peptide within membranes (*30*). The binding isotherms of the three diastereomers with PE/PG vesicles are straight lines, which indicates a simple adhesion process, as opposed to cooperativity in binding. Similar results were obtained with naturally occurring antibacterial peptides such as dermaseptins (*45*, *46*) and cecropins (*47*, *48*).

Secondary Structure of the Diastereomers in PE/PG and PC/Cholesterol Membranes Determined by FTIR Spectroscopy. FTIR spectroscopy was used to determine the secondary structure of the diastereomers within phospholipid membranes. Helical and unordered structures can contribute to the amide I vibration at almost identical wavenumbers, and it is difficult to extract the precise proportion of helix and random coil from IR spectra. However, the exchange of hydrogen with deuterium makes it possible, sometimes, to differentiate α-helical components from random structure, since after deuteration the absorption of the random coil shifts to a greater extent than the helical structure. We therefore examined the IR spectra of the peptides after complete deuteration. Spectra of the amide I region of [D]L^{3,4,8,10}-K$_3$L$_8$W(m), [D]L^{3,4,8,10}-K$_5$L$_6$W(m), and [D]L^{3,4,8,10}-K$_7$L$_4$W-(m) bound to PE/PG (7:3 w/w) multibilayers are shown in Figures 2A, 3A, and 4A, respectively. The spectrum of the amide I region of [D]L^{3,4,8,10}-K$_3$L$_8$W(m) bound to the zwitterionic PC/cholesterol (10:1 w/w) multibilayers was identical to that observed with PE/PG and therefore was not shown. [D]L^{3,4,8,10}-K$_5$L$_6$W(m) and [D]L^{3,4,8,10}-K$_7$L$_4$W(m) do not bind PC/cholesterol and therefore were not examined. Second-derivative spectra accompanied by 13-data point Savitsky−Golay smoothing were calculated to identify the positions of the component bands in the spectra and are given in the corresponding B panels of Figures 2−4. These wavenumbers were used as initial parameters for curve fitting with Gaussian component peaks. Deconvolution of the amide

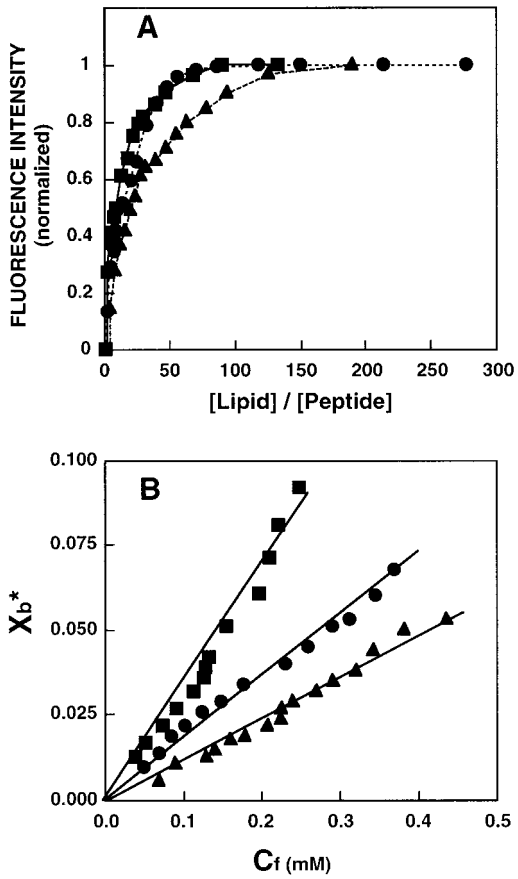

FIGURE 1: (A) Increase in the fluorescence of [D]$L^{3,4,8,10}$-K_3L_8W-(m), [D]$L^{3,4,8,10}$-K_5L_6W(m), and [D]$L^{3,4,8,10}$-K_7L_4W(m) (0.5 μM total concentration) upon titration with PE/PG vesicles, with the excitation wavelength set at 280 nm and emission at 340 nm. The experiment was performed at 25 °C in PBS. (B) Binding isotherm derived from panel A by plotting X_b* (extent of binding) vs C_f (free peptide). Calculations of X_b* and C_f were performed as described in Materials and Methods. Designations are as follows: (■) [D]$L^{3,4,8,10}$-K_3L_8W(m), (●) [D]$L^{3,4,8,10}$-K_5L_6W(m), and (▲) [D]-$L^{3,4,8,10}$-K_7L_4W(m).

Table 3: Partition Coefficients of the Diastereomers As Determined from the Initial Slopes of the Binding Isotherms

sample	lipid type	K_p* (M^{-1})
[D]$L^{3,4,8,10}$-K_3L_8W(m)	PE/PG	$(2.8 \pm 0.6) \times 10^5$
[D]$L^{3,4,8,10}$-K_5L_6W(m)	PE/PG	$(2.1 \pm 0.3) \times 10^5$
[D]$L^{3,4,8,10}$-K_7L_4W(m)	PE/PG	$(1.1 \pm 0.4) \times 10^5$

I region was performed using these Gaussian component peaks, and the results are summarized in Table 4. Assignment of the different secondary structures to the different amide I regions was calculated according to the values taken from Jackson and Mantsch (*49*). The amide I region between 1648 and 1660 cm^{-1} is characteristic of an α-helical structure, and the amide I regions from 1640 to 1648 cm^{-1} and from 1660 to 1670 cm^{-1} are characteristic of unordered and 3_{10}-helix, respectively. The assignment of the amide I region between 1670 and 1680 cm^{-1} remains uncertain. Previous studies have correlated this region with β-turns (*50*), possibly sterically constrained non-hydrogen-bonded amide C═O groups within turns (*51*), or the high-frequency β-sheet component (*52*), which arises as a result of transition dipole coupling (*53*). The results reveal large differences between the secondary structure of the diastereomers. Whereas [D]$L^{3,4,8,10}$-K_3L_8W-(m) adopts predominantly (~88%) an α-helical structure

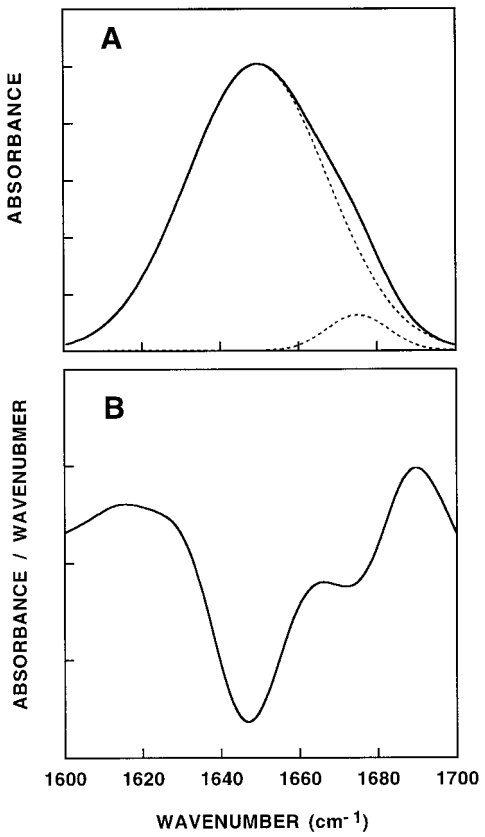

FIGURE 2: FTIR spectra deconvolution of the fully deuterated amide I band (1600−1700 cm^{-1}) of [D]$L^{3,4,8,10}$-K_3L_8W(m) (A) and its second derivatives (B). The component peaks are the result of curve fitting using a Gaussian line shape. The amide I frequencies characteristic of the various secondary structure elements were taken from Jackson and Mantsch (*49*). The sums of the fitted components superimpose on the experimental amide I region spectra. In panel A, the solid line represents the experimental FTIR spectra after Savitzky−Golay smoothing and the dashed lines represent the fitted components. A 100:1 lipid:peptide molar ratio was used.

when bound to either PC or PE/PG membranes, [D]$L^{3,4,8,10}$-K_5L_6W(m) adopts a 3_{10}-helix (40%) and an unordered structure (60%), and [D]$L^{3,4,8,10}$-K_7L_4W(m) is practically unordered (~80%) in PE/PG phospholipid membranes.

Orientation of the Phospholipid Membrane and the Effect of Peptide Binding on the Acyl Chain Order. Polarized ATR-FTIR was used to determine the orientation of the lipid membrane. The symmetric [$\upsilon_{sym}(CH_2) \sim 2850$ cm^{-1}] and the antisymmetric [$\upsilon_{antisym}(CH_2) \sim 2920$ cm^{-1}] vibrations of lipid methylene C−H bonds are perpendicular to the molecular axis of a fully extended hydrocarbon chain. Thus, measurements of the dichroism of infrared light absorbance can reveal the order and orientation of the membrane sample relative to the prism surface. Figure 5A shows an example of the ATR dichroism spectra of parallel and perpendicular polarized ATR-FTIR absorbance spectra between 2800 and 3000 cm^{-1} of PE/PG multibilayers alone, and Figure 5B shows the spectra incorporated with [D]$L^{3,4,8,10}$-K_3L_8W(m). Table 5 shows the calculated *R* values and their corresponding *f* values based on the stronger $\upsilon_{antisym}(CH_2)$. Similar values were obtained when $\upsilon_{sym}(CH_2)$ was used instead (data not shown), as previously found by others (*35*). *R* values based on the stronger $\upsilon_{antisym}(CH_2)$ were 1.38 ± 0.02 for the PE/PG phospholipid membrane. The data indicate that the phospholipid membrane is well-ordered. Similar results were

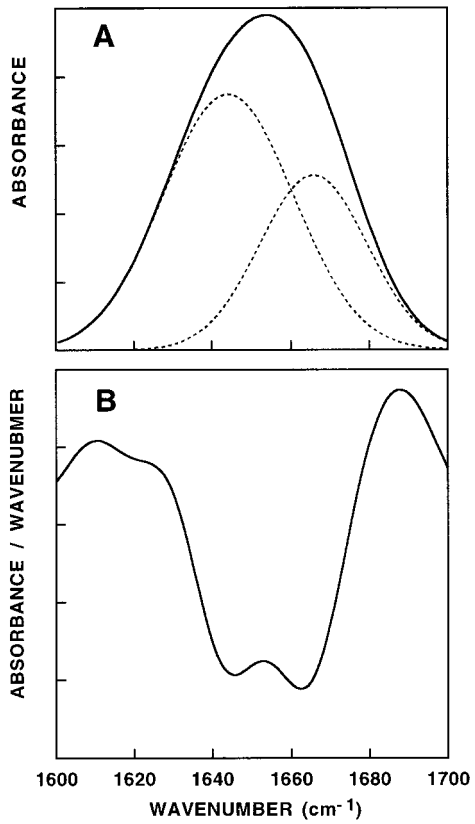

FIGURE 3: FTIR spectra deconvolution of the fully deuterated amide I band (1600−1700 cm^{-1}) of [D]$L^{3,4,8,10}$-K_5L_6W(m) (A) and its second derivatives (B). Details are as described in the legend of Figure 2. A 100:1 lipid:peptide molar ratio was used.

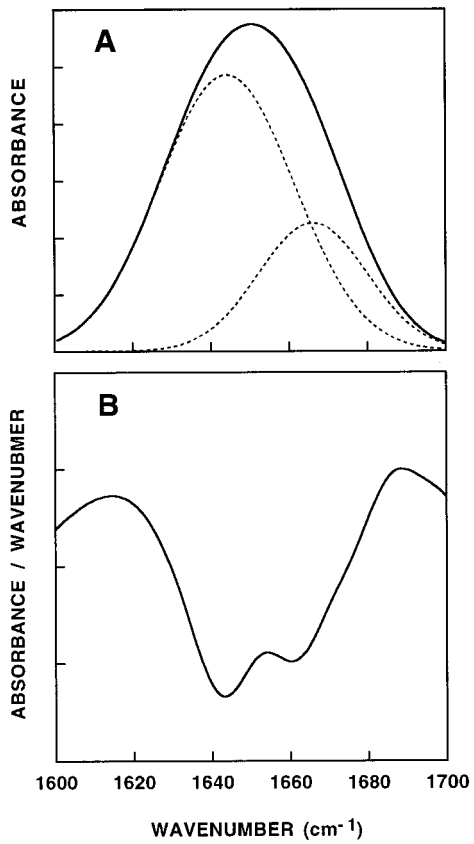

FIGURE 4: FTIR spectra deconvolution of the fully deuterated amide I band (1600−1700 cm^{-1}) of [D]$L^{3,4,8,10}$-K_7L_4W(m) (A) and its second derivatives (B). Details are as described in the legend of Figure 2. A 100:1 lipid:peptide molar ratio was used.

obtained by others (*32*, *35*, *54*, *55*). On the basis of the dichroic ratio of lipid stretching, the corresponding orientation order parameter, *f*, was calculated to be 0.44 ± 0.02 for the PE/PG phospholipid membranes. The observed antisymmetric and symmetric peaks at 2921.9 ± 0.2 and 2852.7 ± 0.3 cm^{-1}, respectively (Figure 5A), indicate that the membranes were predominantly in a liquid-crystalline phase (*35*, *56*), like biological cell membranes. Thus, the lipid multibilayer used in our study was well-oriented and in a liquid-crystalline phase.

The effect of the diastereomers on the multibilayer acyl chain order can be estimated by comparing the CH_2 stretching dichroic ratio of pure phospholipid multibilayers with that obtained with membrane-bound peptide (Table 5). The incorporation of [D]$L^{3,4,8,10}$-K_3L_8W(m) and [D]$L^{3,4,8,10}$-K_5L_6W-(m) into PE/PG phospholipid membranes had a similar large disrupting effect on the acyl chain order. Only a slight increase in the *R* value was observed with [D]$L^{3,4,8,10}$-K_7L_4W-(m), indicating a minor disruption of the acyl chain order.

Orientation of the Peptides in the Membrane Determined by Tryptophan-Quenching Experiments. A tryptophan residue present in the sequence of a protein or a peptide can serve as an intrinsic probe for the localization of the peptide within a membranes. To estimate the orientation and depth of penetration of the diastereomers, we used the three analogues of each group, in which one tryptophan was located in the middle or the N- or C-terminus of the peptides. The peptides were mixed with phospholipids that contained Br, a quencher of tryptophan fluorescence with an r^6 dependence and an apparent R_0 of 9 Å (*40*). Bromo lipids [1-palmitoyl-2-(dibromostearoyl)phosphatidylcholine] with bromines at the 6,7-, 9,10-, and 11,12-positions were used as a molecular ruler. The peptide:lipid molar ratio in these experiments was kept low (1:120). At this peptide:lipid ratio, the wild-type peptides, [D]$L^{3,4,8,10}$-K_3L_8, [D]$L^{3,4,8,10}$-K_5L_6, and [D]$L^{3,4,8,10}$-K_7L_4, did not induce vesicle leakage (*26*). Figure 6 shows an example of the spectra obtained with the different lipid compositions for [D]$L^{3,4,8,10}$-K_5L_6W(c). In all tryptophan-quenching spectra, a shoulder around 355 nm was observed which might suggest the coexistence of membrane-bound and free peptide. However, at the lipid:peptide molar ratio that was used (120:1), the amount of free peptide is probably negligible since maximal binding occurs (Figure 1). Furthermore, even at higher lipid:peptide molar ratios of 200:1 and 300:1, similar spectra were obtained (data not shown). Figure 7 shows the percentage of tryptophan quenching of all the peptides versus the type of brominated phospholipids that were used. With all analogues, the largest quenching of tryptophan fluorescence was observed with 9,10-Br-PC/PE/PG vesicles followed by 6,7-Br-PC/PE/PG. Less quenching was observed with 11,12-Br-PC/PE/PG. In most cases, no significant difference was observed when tryptophan was located in the N-terminus, the C-terminus, or the middle of the peptides. However, it should be noticed that a reduced level of quenching of tryptophan fluorescence was observed with 6,7-Br-PC/PE/PG when tryptophan was positioned in the middle of the peptides, indicating a slight difference in the depth of penetration depending on the position of the tryptophan. When the interface seeking properties of tryptophan are considered (*57*), the high level of quenching

Table 4: Assignments, Wavenumbers (υ), and Relative Areas of the Component Peaks Determined from the Deconvolution of the Amide I Bands of the Peptides Incorporated into PE/PG (7:3 w/w) and PC/Cholesterol (10:1 w/w) Liposomes[a]

	[D]$L^{3,4,8,10}$-K_3L_8W(m)		[D]$L^{3,4,8,10}$-K_5L_6W(m)		[D]$L^{3,4,8,10}$-K_7L_4W(m)	
assignment	υ (cm^{-1})	area (%)	υ (cm^{-1})	area (%)	υ (cm^{-1})	area (%)
PE/PG						
α-helix	1649 ± 1	88 ± 3				
random coil			1643 ± 1	60 ± 4	1644 ± 1	76 ± 3
3_{10}-helix			1666 ± 1	40 ± 4	1666 ± 1	24 ± 3
β-turn/β-sheet	1674 ± 1	12 ± 3				
PC/cholesterol						
α-helix	1649 ± 1	86 ± 2				
random coil						
3_{10}-helix						
β-turn/β-sheet	1674 ± 1	14 ± 2				

[a] A 1:100 peptide:lipid molar ratio was used. Relative area values are given as means ± the standard deviation.

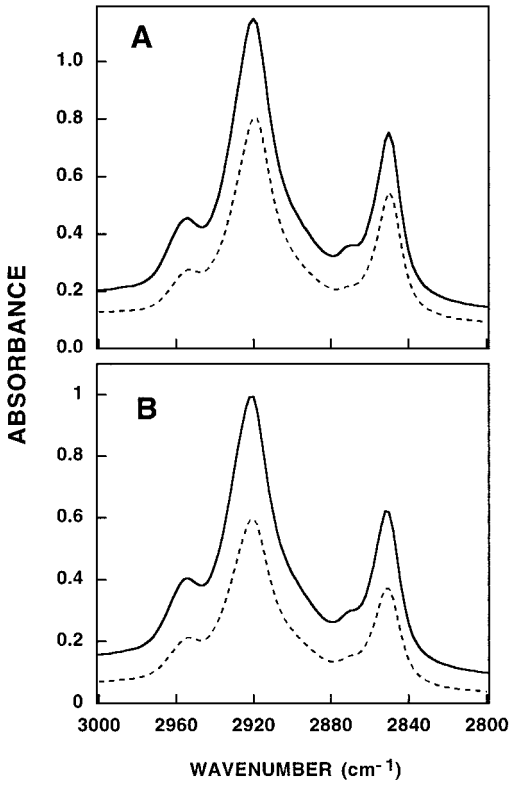

FIGURE 5: ATR dichroism spectra of parallel and perpendicularly polarized ATR-FTIR absorbance spectra between 3000 and 2800 cm^{-1} for the lipid CH_2 symmetric and antisymmetric vibration of PE/PG (7:3 w/w) multibilayers alone (A) or incorporated with [D]-$L^{3,4,8,10}$-K_3L_8W(m) (B). The top line is for the parallel component, and the bottom line is for the perpendicular component.

Table 5: Dichroic Ratios and Order Parameters of Phospholipid Multibilayers[a]

peptides	R of $\upsilon_{antisym}(CH_2)$	f
PE/PG	1.38 ± 0.02	0.44 ± 0.02
PE/PG and [D]$L^{3,4,8,10}$-K_3L_8W(m)	1.57 ± 0.04	0.30 ± 0.04
PE/PG and [D]$L^{3,4,8,10}$-K_5L_6W(m)	1.53 ± 0.06	0.32 ± 0.03
PE/PG and [D]$L^{3,4,8,10}$-K_7L_4W(m)	1.44 ± 0.04	0.39 ± 0.03

[a] A 1:100 peptide:lipid molar ratio was used.

observed with 9,10-Br-PC/PE/PG suggests that the peptide's conformation is involved in forcing the tryptophan residue to penetrate into the acyl chain region. These results suggest that upon binding to vesicles, the diastereomers are located within the acyl chain region, parallel to the surface of the membrane.

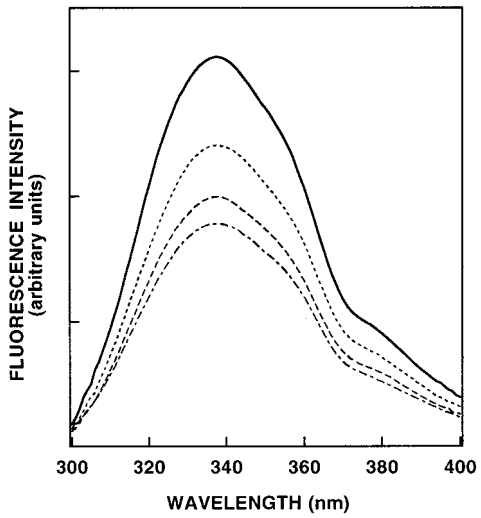

FIGURE 6: Examples of spectra obtained from tryptophan-quenching experiments using brominated phospholipids. Tryptophan fluorescence spectra of [D]$L^{3,4,8,10}$-K_5L_6W(c) in the presence of SUV composed of PC/PE/PG (2.5:4.5:3 w/w) and containing either 6,7-Br-PC, 9,10-Br-PC, or 11,12-Br-PC. The excitation wavelength was set at 280 nm, and emission was scanned from 300 to 400 nm. Designations from the upper line to the lower line are as follows: PC/PE/PG, 11,12-Br-PC/PE/PG, 6,7-Br-PC/PE/PG, and 9,10-Br-PC/PE/PG.

Orientation of [D]$L^{3,4,8,10}$-K_3L_8W(m) in the Membrane Determined by ATR-FTIR Spectroscopy. FTIR experiments revealed that only [D]$L^{3,4,8,10}$-K_3L_8W(m) can adopt an α-helical structure in the membrane, and therefore, its orientation could be determined by using polarized ATR-FTIR in both PC and PE/PG. The dichroic ratio value, R, was calculated from the amide I absorption at 1649 cm^{-1} in the polarized spectra and was found to be 1.55 ± 0.02 in both types of membranes. The corresponding order parameter, f, assuming $\alpha = 27°$ (*35*, *37*), was calculated as described in Materials and Methods and was found to be −0.15. When $\alpha = 39°$ (*38*, *39*), the order parameter was found to be −0.25. Negative order parameters are observed for helices oriented nearly parallel to the membrane surface (*36*). These results confirm those obtained in the tryptophan-quenching experiments.

DISCUSSION

Recently, we reported a study on a new group of diastereomeric antimicrobial peptides having several advantages over native antimicrobial peptides, e.g., stability in

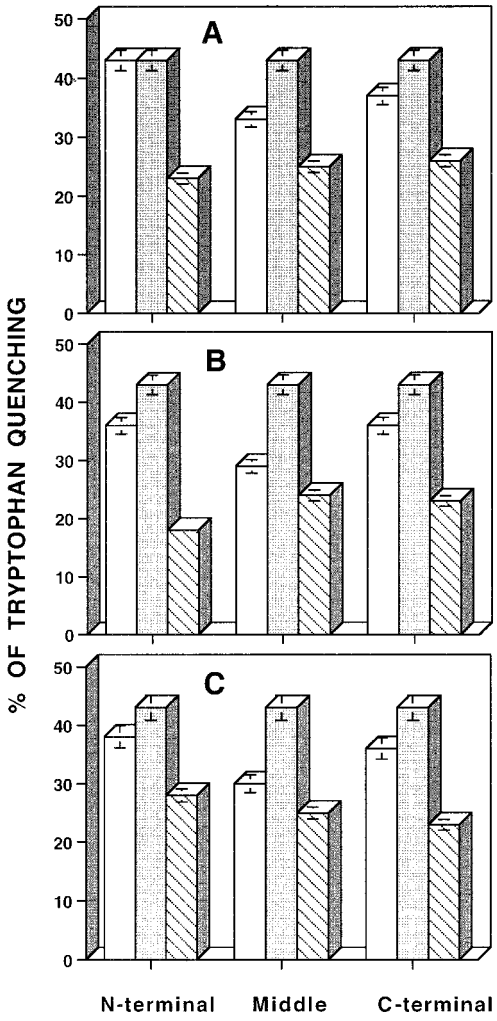

FIGURE 7: Percentage of tryptophan quenching using brominated phospholipids. The percentage of quenching was calculated according to the tryptophan fluorescence spectra obtained in the presence of PC/PE/PG (2.5:4.5:3 w/w) liposomes, or in the presence of Br-PC/PE/PG liposomes containing either 25% 6,7-Br-PC, 9,-10-Br-PC, or 11,12-Br-PC. The excitation wavelength was set at 280 nm, and emission was scanned from 300 to 400 nm. Panel A shows the results for [D]$L^{3,4,8,10}$-K_3L_8W(n), -(m), and -(c), panel B for [D]$L^{3,4,8,10}$-K_5L_6W(n), -(m), and -(c), and panel C for [D]$L^{3,4,8,10}$-K_7L_4W(n), -(m), and -(c). In every three-column group, the first column stands for the result obtained with 6,7-Br-PC/PE/PG, the second column with 9,10-Br-PC/PE/PG, and the third column with 11,12-Br-PC/PE/PG.

serum and reduced cytotoxic effects (*26*). However, compared with native antimicrobial peptides about which much information of their mode of action is known, the structure and organization of diastereomeric antimicrobial peptides in membranes have not been investigated. This information is important for shedding light on their mode of action, which would help to develop efficient peptide antibiotics for therapeutic use.

The results presented here will be discussed considering three interesting findings: (i) diastereomers with different number of positive charges, and substantially different antibacterial and hemolytic activities bind similarly to negatively charged phospholipid membranes; (ii) despite the incorporation of 33% D-amino acids along the peptide backbone, a diastereomeric peptide can still adopt a predominantly α-helical structure when bound to the membrane; and (iii) despite their different structures in the membrane and different biological potencies, all the peptides insert similarly into the membrane and are oriented parallel to the membrane surface.

Studies with naturally occurring amphipathic α-helical peptides and their analogues showed a direct correlation between the ability of a peptide to bind and disrupt target membranes and its antimicrobial and hemolytic activity. Here we found that the three types of diastereomers bind and insert similarly to negatively charged membranes, although their antibacterial activities are not the same. In addition, the only peptide that can bind (blue shift in tryptophan fluorescence) and permeate (*26*) zwitterionic membrane is the K_3L_8W derivative, which is also the only one that can induce hemolysis of red blood cells. The other two diastereomers could neither bind (no change in tryptophan fluorescence) nor induce leakage of zwitterionic membranes at concentrations more than 100-fold higher than those needed to induce leakage from negatively charged membranes (*26*). The nonhemolytic activity of $L^{3,4,8,10}$-K_5L_6W(m) and [D]$L^{3,4,8,10}$-K_7L_4W(m) can be attributed to their inability to bind zwitterionic phospholipids. The repulsion of the diastereomers from the zwitterionic PC membrane, because of its positively charged choline group, prevents them from penetrating into the hydrophobic region of the bilayers to create an active secondary structure. These results are different from what has been observed with native amphipathic α-helical antimicrobial peptides such as magainin, dermaseptin B, dermaseptin S, cecropin B, and cecropin P, which are nonhemolytic but still can bind and permeate zwitterionic membranes, although with a 10-fold higher concentration compared with that needed for negatively charged membranes (*45*, *48*, *58*). This may explain in part their inability to lyse red blood cells, in which the outer leaflet is composed of predominantly zwitterionic (PC) and sphingomyelin phospholipids (*44*). However, they can lyse the bacterial surface that contains lipopolysaccharides (LPS, in Gram-negative bacteria) and polysaccharides (teichoic acids, in Gram-positive bacteria), as well as their cytoplasmic membranes that contain phosphatidylglycerol (PG), all of which are negatively charged. The inability of the diastereomers to bind (or only weakly bind) zwitterionic membranes can be another advantage of this group of peptides for in vivo application, since they will have a reduced ability to bind mammalian cells (that contain zwitterionic membranes on their outer leaflet) compared with native antimicrobial peptides or de novo-designed L-amino acid amphipathic α-helical antimicrobial peptides.

Electrostatic and hydrophobic interactions between the diastereomers and the phospholipid membranes play a major role in their binding to membranes. All the diastereomers carry a net positive charge. However, whereas [D]$L^{3,4,8,10}$-K_5L_6W(m) and [D]$L^{3,4,8,10}$-K_7L_4W(m) bind only to negatively charged phospholipid membranes, [D]$L^{3,4,8,10}$-K_3L_8W(m) can bind to both negatively charged and zwitterionic membranes, indicating that its binding is mostly governed by hydrophobic interactions. The partition coefficients of all the diastereomers with PE/PG membranes were on the same order of magnitude (10^5 M^{-1}) (Table 3). [D]$L^{3,4,8,10}$-K_3L_8W(m) has the highest affinity, followed by $L^{3,4,8,10}$-K_5L_6W(m). However, the difference between the affinities of $L^{3,4,8,10}$-K_5L_6W(m) and $L^{3,4,8,10}$-K_7L_4W(m) cannot explain the finding that $L^{3,4,8,10}$-K_7L_4W(m) is more than 10-fold less potent than $L^{3,4,8,10}$-

K_5L_6W(m) with most tested bacteria. This suggests that electrostatic interactions are the main cause for the high affinity of the peptides for negatively charged membranes; however, membrane binding is not necessarily associated with membrane disruption. Interestingly, despite a substantial decrease in the antibacterial activity of [D]$L^{3,4,8,10}$-K_7L_4W-(m) compared with the other two, it is as active as they are on *B. subtillis*. However, this bacterium is highly susceptible to many cytolytic peptides.

The structures of [D]$L^{3,4,8,10}$-K_3L_8W(m), [D]$L^{3,4,8,10}$-K_5L_6W-(m), and [D]$L^{3,4,8,10}$-K_7L_4W(m) in phospholipid membranes were determined by using FTIR spectroscopy. The two potent antimicrobial diastereomers [D]$L^{3,4,8,10}$-K_3L_8W(m) and [D]-$L^{3,4,8,10}$-K_5L_6W(m) adopt α-helix (∼90%) and 3_{10}-helix (40%) structures, respectively. In contrast, [D]$L^{3,4,8,10}$-K_7L_4W(m), which has very low antimicrobial activity, is predominantly unordered. These results indicate that there is a need for an ordered structure, which in the case of the diastereomeric peptides is either an α-helix or 3_{10}-helix, to confer high antibacterial activity. The conformation of the diastereomers in their membrane-bound state is determined by a balance between forces that favor an unordered structure and forces that favor a defined one. Forces that favor an unordered structure include (i) repulsive forces between positively charged lysines, which favor an extended unfolded state (*59*, *60*), which can be partially neutralized by the negative charges of the phospholipid headgroups; and (ii) the destabilizing effect of D-amino acids incorporated into an α-helical structure. Previous studies have shown that incorporating D-amino acid or even an adjacent pair of D-amino acids caused a local change in structure and flexibility of α-helical structures when the peptides are in solution (*61*−*64*). Forces that influence the formation of a specific structure include hydrophobic interactions between the nonpolar amino acids and the phospholipid hydrocarbon layer. Therefore, the ability of the diastereomers to adopt a secondary structure in the membrane, despite the existence of D-amino acids, can only be attributed to the hydrophobic interactions. The free energy of the hydrophobic stretches of amino acids found in [D]$L^{3,4,8,10}$-K_3L_8W(m) drives the formation of the α-helix in the apolar membrane milieu. This tendency compensates for the destabilizing effect of the D-amino acids. The addition of positively charged lysines leads to disruption of the α-helical structure with [D]$L^{3,4,8,10}$-K_5L_6W(m), and to almost a complete elimination of the helical structure with [D]-$L^{3,4,8,10}$-K_7L_4W(m). Once a hydrophobic diastereomer is bound to zwitterionic membranes, it adopts the same secondary structure as in negatively charged membranes (Table 4). This suggests that it lyses zwitterionic and negatively charged phospholipids via the same mechanism.

Although electrostatic interactions between the positively charged diastereomers and the negatively charged phospholipid membranes seem to have an important role in the initial interactions and selectivity, biological activity appears to be driven by the hydrophobic interactions between the helix nonpolar surface and the hydrophobic core of the lipid bilayer. Polarized ATR-FTIR spectroscopy revealed that incorporating the diasteriomers into negatively charged membranes disrupted the acyl chain order (Table 5), indicating a need for a threshold of hydrophobicity and a helical structure to affect the acyl chain order. Incorporation of [D]-$L^{3,4,8,10}$-K_3L_8W(m) and [D]$L^{3,4,8,10}$-K_5L_6W(m) into PE/PG phospholipid membranes had similar large effect on the acyl chain order. [D]$L^{3,4,8,10}$-K_7L_4W(m) increased the *R* value only slightly, indicating a minor disruption of the acyl chain order.

We found that all the peptides penetrate into the membrane to similar depths, as determined in the quenching experiments with brominated phospholipids (Figure 7). [D]$L^{3,4,8,10}$-K_7L_4W-(m), which is mostly unordered and has very low antimicrobial activity, penetrates into the acyl chain region like the highly active [D]$L^{3,4,8,10}$-K_3L_8W(m) and [D]$L^{3,4,8,10}$-K_5L_6W(m). These results further indicate that membrane penetration is not sufficient by itself for membrane lysis, but rather, a defined structure is needed such as an α-helix that causes the pointing of all the hydrophobic amino acids into one surface that can interact and disrupt the lipid order. The findings that similar depths of penetration were observed irrespective of whether tryptophan was located at the center or the N- or C-terminus of the peptides suggest that the peptides are oriented parallel to the surface of the membrane. This orientation was confirmed by ATR-FTIR studies with the helical peptide [D]$L^{3,4,8,10}$-K_3L_8W(m), which revealed negative order parameter characteristics of peptides that lie parallel to the membrane surface.

Our results with the model diastereomers support a "carpet-like" mechanism of bacterial lysis by this group of peptides (*4*, *45*, *65*−*67*). The carpet mechanism describes a situation in which the diastereomers bind to the membrane and subsequently cover and dissolve it like a detergent. Hydrophobic and positively charged amino acids possibly play different roles in the steps involved in this model as follows: (i) the positive charges enable the diastereomers to selectively bind negatively charged phospholipids (Table 3 and Figure 1); (ii) hydrophobic amino acids lead to penetration of the diastereomers into the acyl chain and drive the formation of the helical structure (Figures 2 and 5); (iii) the molecule is reorganized so that the positive charges of the basic amino acids can interact with the negatively charged phospholipid headgroups or water molecules, and the hydrophobic residues can interact with the hydrophobic core of the membrane; and (iv) the membrane is disintegrated by forcing the alkyl chains of the phospholipids apart (Table 5), and thus disrupting the lipid bilayer structure. The last step in this model probably occurs only after a high peptide: lipid molar ratio is reached.

In summary, the distinct characteristics of hydrophobic and positively charged amino acids determine the selective antimicrobial activity of the diastereomers by affecting the membrane binding, structure, depth of penetration, and disruption. Further studies on the parameters that affect the interaction and organization of the diastereomers in the membrane may lead to the development of new antibiotics that would overcome bacteria resistance.

REFERENCES

1. John, C. C. (1999) *N. Engl. J. Med. 341*, 207−208.
2. Chen, D. K., McGeer, A., De Azavedo, J. C., and Low, D. E. (1999) *N. Engl. J. Med. 341*, 233−239.
3. Boman, H. G. (1995) *Annu. Rev. Immun. 13*, 61−92.
4. Shai, Y. (1995) *Trends Biochem. Sci. 20*, 460−464.
5. Hoffmann, J. A. (1995) *Curr. Opin. Immunol. 7*, 4−10.
6. Nicolas, P., and Mor, A. (1995) *Annu. Rev. Microbiol. 49*, 277−304.
7. Hancock, R. E., and Lehrer, R. (1998) *Trends Biotechnol. 16*, 82−88.

8. Lehrer, R. I., and Ganz, T. (1999) *Curr. Opin. Immunol. 11*, 23−27.
9. Hoffmann, J. A., Kafatos, F. C., Janeway, C. A., and Ezekowitz, R. A. (1999) *Science 284*, 1313−1318.
10. Segrest, J. P., De, L. H., Dohlman, J. G., Brouillette, C. G., and Anantharamaiah, G. M. (1990) *Proteins 8*, 103−117.
11. Epand, R. M. (1993) *The Amphipathic Helix*, CRC Press, Boca Raton, FL.
12. Steiner, H., Hultmark, D., Engstrom, A., Bennich, H., and Boman, H. G. (1981) *Nature 292*, 246−248.
13. Zasloff, M. (1987) *Proc. Natl. Acad. Sci. U.S.A. 84*, 5449−5453.
14. Mor, A., Nguyen, V. H., Delfour, A., Migliore, S. D., and Nicolas, P. (1991) *Biochemistry 30*, 8824−8830.
15. Dhople, V. M., and Nagaraj, R. (1993) *Biosci. Rep. 13*, 245−250.
16. Habermann, E., and Jentsch, J. (1967) *Hoppe Seyler's Z. Physiol. Chem. 348*, 37−50.
17. Lazarovici, P., Primor, N., and Loew, L. M. (1986) *J. Biol. Chem. 261*, 16704−16713.
18. Shai, Y., Fox, J., Caratsch, C., Shih, Y. L., Edwards, C., and Lazarovici, P. (1988) *FEBS Lett. 242*, 161−166.
19. Mignogna, G., Simmaco, M., Kreil, G., and Barra, D. (1993) *EMBO J. 12*, 4829−4832.
20. Kreil, G. (1994) *J. Biol. Chem. 266*, 6264−6270.
21. Killian, J. A. (1992) *Biochim. Biophys. Acta 1113*, 391−425.
22. Shai, Y., and Oren, Z. (1996) *J. Biol. Chem. 271*, 7305−7308.
23. Oren, Z., and Shai, Y. (1997) *Biochemistry 36*, 1826−1835.
24. Blondelle, S. E., and Houghten, R. A. (1992) *Biochemistry 31*, 12688−12694.
25. Cornut, I., Buttner, K., Dasseux, J. L., and Dufourcq, J. (1994) *FEBS Lett. 349*, 29−33.
26. Oren, Z., Hong, J., and Shai, Y. (1997) *J. Biol. Chem. 272*, 14643−14649.
27. Merrifield, R. B., Vizioli, L. D., and Boman, H. G. (1982) *Biochemistry 21*, 5020−5031.
28. Bartlett, G. R. (1959) *J. Biol. Chem. 234*, 466−468.
29. Rizzo, V., Stankowski, S., and Schwarz, G. (1987) *Biochemistry 26*, 2751−2759.
30. Schwarz, G., Gerke, H., Rizzo, V., and Stankowski, S. (1987) *Biophys. J. 52*, 685−692.
31. Beschiaschvili, G., and Seelig, J. (1990) *Biochemistry 29*, 52−58.
32. Gazit, E., Miller, I. R., Biggin, P. C., Sansom, M. S. P., and Shai, Y. (1996) *J. Mol. Biol. 258*, 860−870.
33. Surewicz, W. K., Mantsch, H. H., and Chapman, D. (1993) *Biochemistry 32*, 389−394.
34. Harrick, N. J. (1967) *Internal Reflection Spectroscopy*, Interscience, New York.
35. Ishiguro, R., Kimura, N., and Takahashi, S. (1993) *Biochemistry 32*, 9792−9797.
36. Tamm, L. K., and Tatulian, S. A. (1997) *Q. Rev. Biophys. 30*, 365−429.
37. Rothschild, K. J., and Clark, N. A. (1979) *Science 204*, 311−312.
38. Tsuboi, M. (1962) *J. Polym. Sci. 59*, 139−153.
39. Bradbury, E. M., Brown, L., Downie, A. R., Elliott, A., Fraser, R. D. B., and Hanby, W. E. (1962) *J. Mol. Biol. 5*, 230−247.
40. Bolen, E. J., and Holloway, P. W. (1990) *Biochemistry 29*, 9638−9643.
41. De Kroon, A. I., Soekarjo, M. W., De Gier, J., and De Kruijff, B. (1990) *Biochemistry 29*, 8229−8240.
42. Eisenberg, D., Schwarz, E., Komaromy, M., and Wall, R. (1984) *J. Mol. Biol. 179*, 125−142.
43. Shaw, N. (1974) *Adv. Appl. Microbiol. 17*, 63−108.
44. Verkleij, A. J., Zwaal, R. F., Roelofsen, B., Comfurius, P., Kastelijn, D., and Deenen, L. V. (1973) *Biochim. Biophys. Acta 323*, 178−193.
45. Pouny, Y., Rapaport, D., Mor, A., Nicolas, P., and Shai, Y. (1992) *Biochemistry 31*, 12416−12423.
46. Strahilevitz, J., Mor, A., Nicolas, P., and Shai, Y. (1994) *Biochemistry 33*, 10951−10960.
47. Gazit, E., Lee, W. J., Brey, P. T., and Shai, Y. (1994) *Biochemistry 33*, 10681−10692.
48. Gazit, E., Boman, A., Boman, H. G., and Shai, Y. (1995) *Biochemistry 34*, 11479−11488.
49. Jackson, M., and Mantsch, H. H. (1995) *Crit. Rev. Biochem. Mol. Biol. 30*, 95−120.
50. Pezolet, M., Bonenfant, S., Dousscau, F., and Papineau, Y. (1992) *FEBS Lett. 299*, 247−250.
51. Mantsch, H. H., Perczel, A., Hollosi, M., and Fasman, G. D. (1993) *Biopolymers 33*, 201−207.
52. Byler, D. M., and Susi, H. (1986) *Biopolymers 25*, 469−487.
53. Miyazawa, T. (1960) *J. Mol. Spectrosc. 4*, 168−172.
54. Fringeli, U. P., and Günthard, H. H. (1981) *Infrared membrane spectroscopy*, Springer-Verlag, Berlin and Heidelberg, Germany.
55. Yang, P. W., Stewart, L. C., and Mantsch, H. H. (1987) *Biochem. Biophys. Res. Commun. 145*, 298−302.
56. Cameron, D. G., Casal, H. L., Gudgin, E. F., and Mantsch, H. H. (1980) *Biochim. Biophys. Acta 596*, 463−467.
57. Yau, W. M., Wimley, W. C., Gawrisch, K., and White, S. H. (1998) *Biochemistry 37*, 14713−14718.
58. Matsuzaki, K., Harada, M., Funakoshi, S., Fujii, N., and Miyajima, K. (1991) *Biochim. Biophys. Acta 1063*, 162−170.
59. Marqusee, S., Robbins, V. H., and Baldwin, R. L. (1989) *Proc. Natl. Acad. Sci. U.S.A. 86*, 5286−5290.
60. Sung, S. S. (1995) *Biophys. J. 68*, 826−834.
61. Rothemund, S., Beyermann, M., Krause, E., Krause, G., Bienert, M., Hodges, R. S., Sykes, B. D., and Sonnichsen, F. D. (1995) *Biochemistry 34*, 12954−12962.
62. Rothemund, S., Krause, E., Beyermann, M., Dathe, M., Engelhardt, H., and Bienert, M. (1995) *J. Chromatogr. 689*, 219−226.
63. Rothemund, S., Krause, E., Beyermann, M., Bienert, M., Sykes, B. D., and Sonnichsen, F. D. (1996) *Biopolymers 39*, 207−219.
64. Krause, E., Beyermann, M., Dathe, M., Rothemund, S., and Bienert, M. (1995) *Anal. Chem. 67*, 252−258.
65. Oren, Z., and Shai, Y. (1998) *Biopolymers 47*, 451−463.
66. La Rocca, P., Shai, Y., and Sansom, M. S. (1999) *Biophys. Chem. 76*, 145−159.
67. Oren, Z., Lerman, J. C., Gudmundsson, G. H., Agerberth, B., and Shai, Y. (1999) *Biochem. J. 341*, 501−513.

BI991850Y